CERN-ACC-NOTE-2018-0045

2018-01-15

Suitbert.Ramberger@cern.ch

Magnetic Measurements of the Vacuum Vessel for the High-Gradient Four-Cavity Cryomodule

Sotirios Papadopoulos, Suitbert Ramberger, CERN BE-RF

Keywords: SPL, Superconducting RF, magnetic shielding

Summary

This document summarizes the results of magnetic measurements performed on the vacuum vessel for the High-Gradient cryomodule.

1 Introduction

In the framework of the High-Gradient project at CERN, a four 5-cell high beta cavity cryomodule, originally conceived for the SPL is now being manufactured. For reaching high quality factor (Q-factor) and ensuring good RF operation with low probability of quenching and high probability of Q-restoration there is need for good magnetic isolation. For that purpose a warm and a cold magnetic shield have been designed. A contribution to the magnetic shielding is expected also from the vacuum vessel. Magnetic measurements have been performed in order to define the shielding factor of the vacuum vessel and investigate any potential need for demagnetization in case the vessel is partially or completely magnetized.

2 Measurement devices

For the magnetic measurements, a 3-axis fluxgate magnetometer was used (Bartington MAG-03MS1000) along with a power supply and display unit (Magmeter-2) from the same company. This measurement setup offers a field resolution of $1\,\mu\mathrm{T}$ and spatial resolution of $18\,\mathrm{mm}$. Because of the low expected shielding performace and the size of the vacuum vessel (length: $7\,\mathrm{m}$) the aformentioned characteristics were assumed appropriate. In figure 1 both of the devices are shown. For more information refer to [1].

3 Measurement setup

In order to perform measurements in the interior of the vacuum vessel while the top lid is closed the fluxgate was put on a wooden stick with a length of $2.7\,\mathrm{m}$. The wood was chosen for reasons of ease and for its non-magnetic characteristics. The bending of the stick due to the weight of

(a) Three-axis fluxgate magnetometer

(b) Power supply and display unit

Fig. 1: Measurement devices used for measuring the magnetic field around and inside of the vacuum vessel.

the sensor caused a disclocation from the central axis of 2 to 3 cm. Measurements have been taken showing that this offset didn't lead to an error of more than $1\,\mu\mathrm{T}$. Some relative pictures of the measurement process are given in figure 2. The magnetometer was moved in steps of $10\,\mathrm{cm}$ inside the vacuum vessel with few measurements being taken outside for reference (figure 2a). Shorter wooden sticks were used in the vacuum vessel, perpendicular to the magnetometer stick in order to support it and to reduce sagging (figure 2b). The alignment and centering was done manually by a stand that matched the height of the five side openings of the vacuum vessel. The desk was positioned such as to ensure straight movement of the stick (figure 2c).

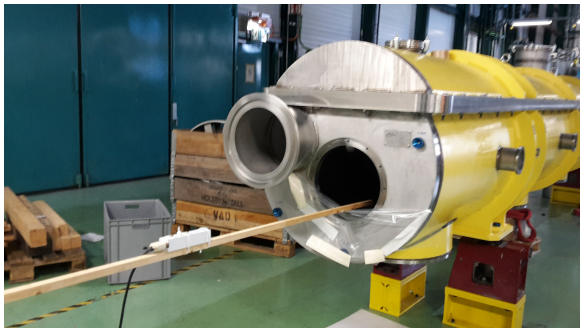

(a)

(b)

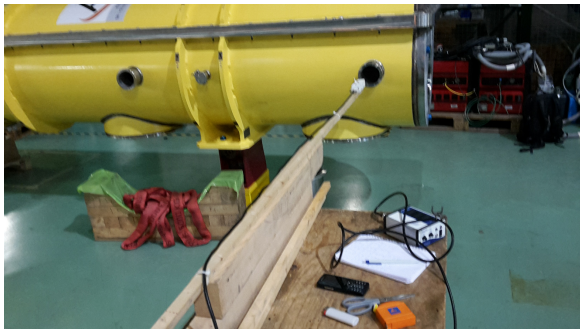

(c)

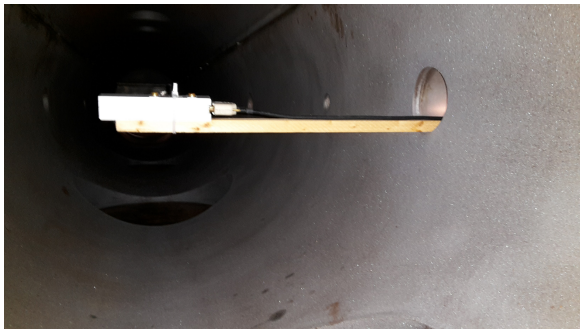

(d)

Fig. 2: Different views and stages of the measurement process

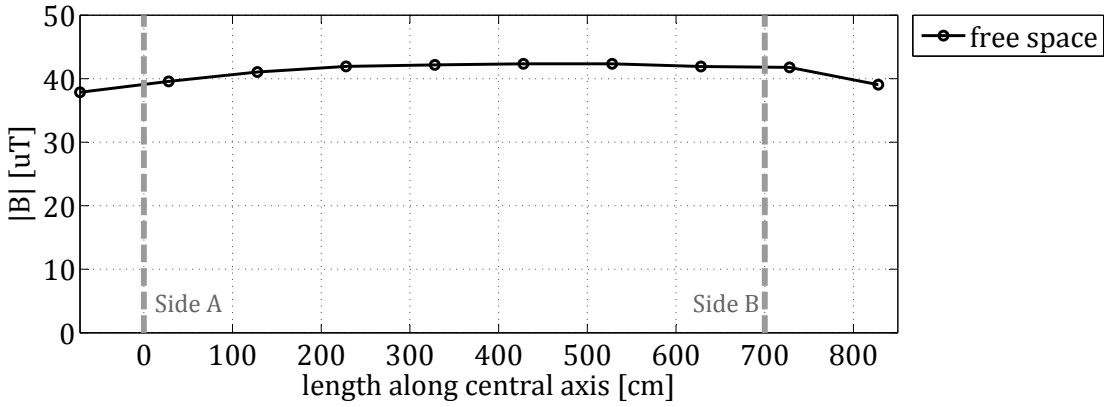

Fig. 3: Measured absolute value of the magnetic field in absence of the vessel at the position of the central axis. The results are expressed in the coordinate system of the vessel defined in figure 4. Sides A and B refer to the position of the two ends of the vessel defined in figure 4a.

4 Measurement results

4.1 Magnetic measurements in absence of the vessel

Figure 4 shows the various axes along which measurements have been taken. The yellow line is the central axis of the vessel and the red lines denote five axes perpendicular to the central axis defined by the positions of the openings at the side of the vessel. At the measurements, the vacuum vessel was standing in building SMI2 at CERN (coord: 46.238886, 6.034890) and it had an orientation with initial north bearing of $301°$. This gives an ambient magnetic field calculated by the World Magnetic Model (WMM) [2] on the axis system of the vacuum vessel of X: $-18.788\,\mu T$, Y: $-41.2\,\mu T$ and Z: $12.22\,\mu T$ (see figure 4 for axis system). Measurements in absence of the vacuum vessel at the location were the vessel will be placed give on average X: $(-17 \pm 1)\,\mu T$, Y: $(-36.5 \pm 1.6)\,\mu T$ and Z: $(10.0 \pm 3.2)\,\mu T$. There is only a small difference between the WMM prediction and the measurements. The measured field is used as a reference. Measurements were taken in absence of the vessel at the same location were the vessel was positioned during the measurements (see figure 3).

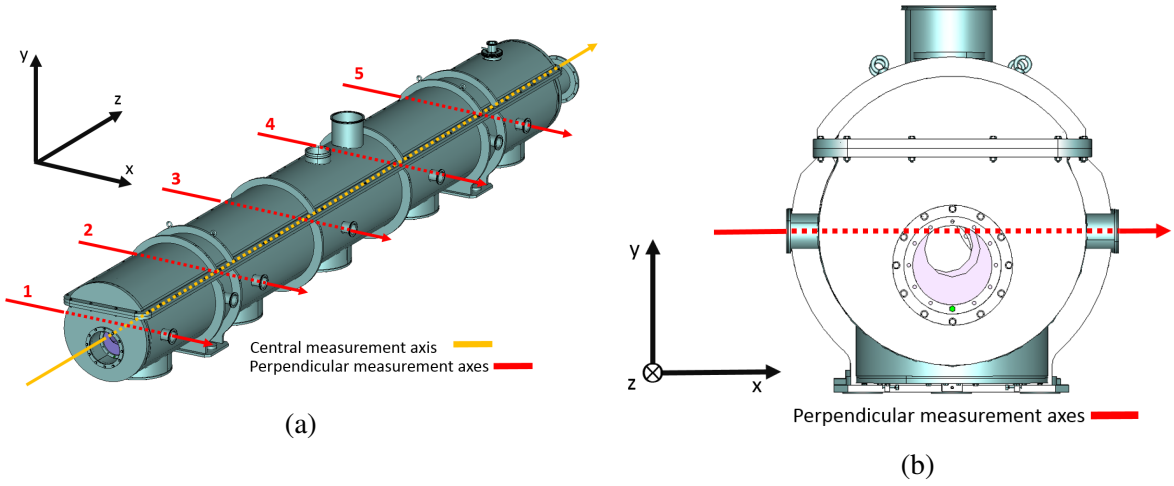

Fig. 4: Geometry of the vacuum vessel and the various axes of measurements

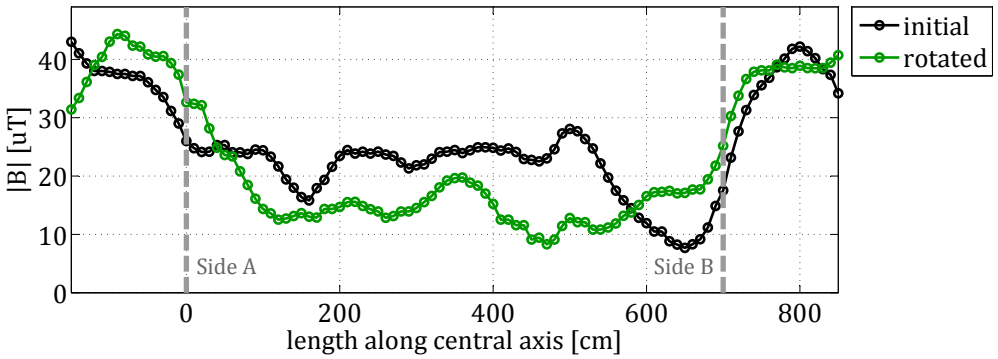

Fig. 5: Measured absolute value of the magnetic field on the central axis of the vessel for the initial orientation and the one rotated by $180°$ around the **y**-axis. The results are displayed in the coordinate system of the vessel defined in figure 4. Sides A and B refer to the two ends of the vessel defined in figure 4a.

5 Measurements on the central axis of the vessel

Measurements are performed on the central axis, in order to define the shielding efficiency of the vessel and compare the magnetic field with and without it. In case the vessel is magnetized, an increase in the magnetic field values is expected inside. The measurements will reveal points where the field values are much higher than the ambient field. However, if the magnetization field is comparable to the ambient field level that penetrates inside the vessel then the measurements will not be able to distinguish between the two. In that case the magnetization field will either enhance or reduce the penetrated field through vectorial superposition and it could give the impression of very high or very low magnetic shielding efficiency. In order to decouple the two effects the field inside the vessel is measured for an initial orientation and one rotated by $180°$. In that way, practically the ambient magnetic field changes orientation around the vessel and information that is invariant to the orientation of the vessel can be extracted as can be shown by the following equations:

$$\left.\begin{array}{l} B_{0^\circ} = B_{mag} + B_{bg} \\ B_{180^\circ} = B_{mag} - B_{bg} \end{array}\right\} B_{mag} = \frac{B_{0^\circ} + B_{180^\circ}}{2} \qquad (1)$$

where B_{0° and B_{180° is the total field for each orientation, B_{bg} is the background ambient field and B_{mag} is the field by permanent magnetization of the vessel. It is shown that an estimation of the B_{mag} can be extracted by the two measurements. Unfortunately since the tank can only be rotated around the **y**-axis, only the **x** and **z** component of the field can be analysed in that way. The **y** component will remain unchanged since the corresponding ambient field component is the same in both orientations, given a uniform ambient magnetic field all over the space surrounding the vessel.

The results are presented in figures 5 to 8. The coordinate system is shown in figure 4 and refers to the vacuum vessel coordinate system for both orientations. The absolute value of the field for the initial and rotated orientation is given in figure 5. One can observe a small magnetization but the field distribution remains the same with an average difference between the two orientations of less than $7\,\mu\mathrm{T}$. It is interesting to observe the field distribution at the two ends of the vessel. The field outside of side A for the initial orientation has the same shape as the field outside of

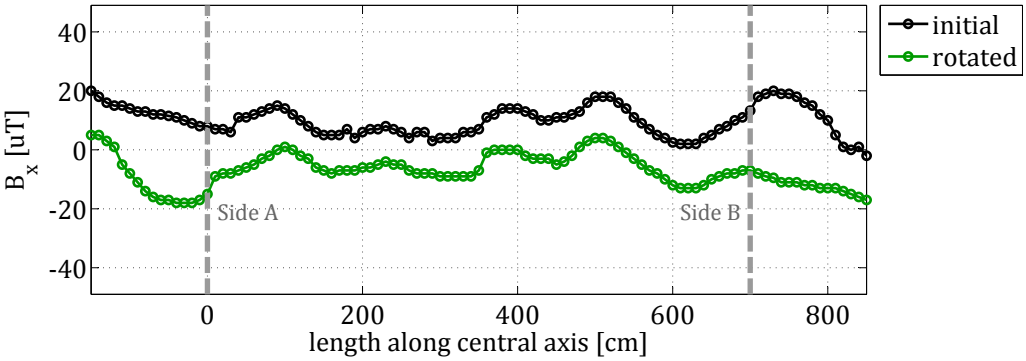

Fig. 6: Measured **x**-component of the magnetic field on the central axis of the vessel for the initial orientation and the one rotated by $180°$ around the **y**-axis. The results are displayed in the coordinate system of the vessel defined in figure 4. Sides A and B refer to the two ends of the vessel defined in figure 4a.

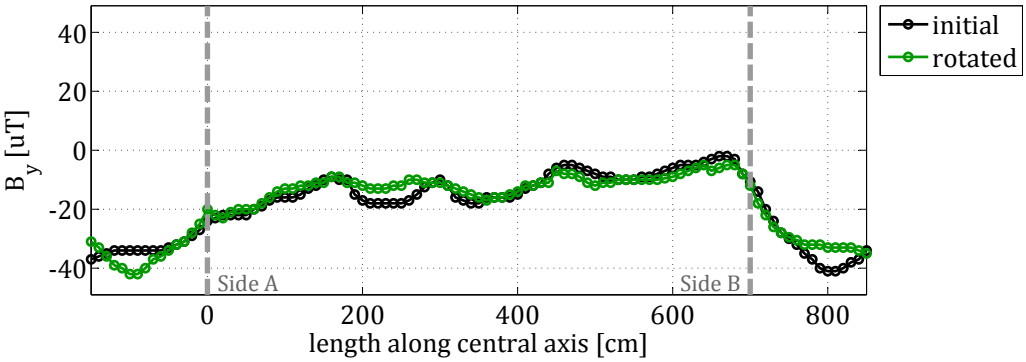

Fig. 7: Measured **x**-component of the magnetic field on the central axis of the vessel for the initial orientation and the one rotated by $180°$ around the **y**-axis. The results are displayed in the coordinate system of the vessel defined in figure 4. Sides A and B refer to the two ends of the vessel defined in figure 4a.

side B in the rotated orientation and vice versa. This means that there is a strong variation in field, sufficiently far away from the vessel. This is the location of the air-conditioning system of the facility.

In order to analyse the characteristics of the field, the different spatial components are examined separately. The measured **x**-component is shown in figure 6. The measurement reveals a pattern which is exactly the same in the two orientations. The fields of initial and rotated orientation have opposite signs as expected for any penetrating field because of the rotation while their shap is rather identical. This means that this contribution to the measured field comes from magnetized parts of the vessel.

As said earlier, the **y**-component of the field is not expected to be any different between the two measurements since the orientation of the **y**-component is not changed with respect to the vessel due to the rotation around the **y**-axis. The measurements are presented in figure 7.

Similarly to the **x**-component, the fields of initial and rotated orientation of the **z**-component have opposite signs (figure 8). The small enhancement in field in the case of the rotated orienta-

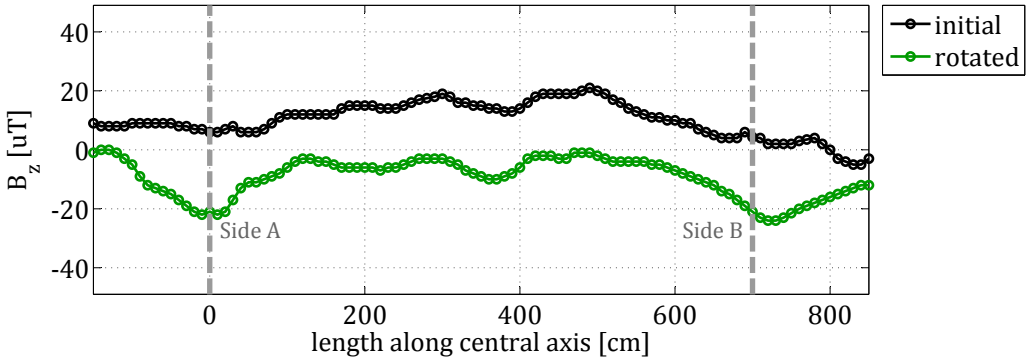

Fig. 8: Measured **z**-component of the magnetic field on the central axis of the vessel for the initial orientation and the one rotated by $180°$ around the **y**-axis. The results are displayed in the coordinate system of the vessel defined in figure 4. Sides A and B refer to the two ends of the vessel defined in figure 4a.

tion around the $380\,\mathrm{cm}$ point is of particular interest. This is the location of the central weld in the circumference of the vessel almost at its center (see figure 9). More precise measurements have been taken in the vicinity of the weld to investigate the impact of its magnetization on the warm magnetic shield which will be situated very close to the inner surface of the vessel. Figure 10 shows the **x** and **y** component of B_{mag} as it was calculated through equation 1.

The contribution of these two components will be given by their vectorial superposition with a mean value of:

$$\langle B_{mag} \rangle = \frac{1}{l} \int_0^l \sqrt{B^2_{mag\ x} + B^2_{mag\ z}}\, dl = 13\ \mu T$$

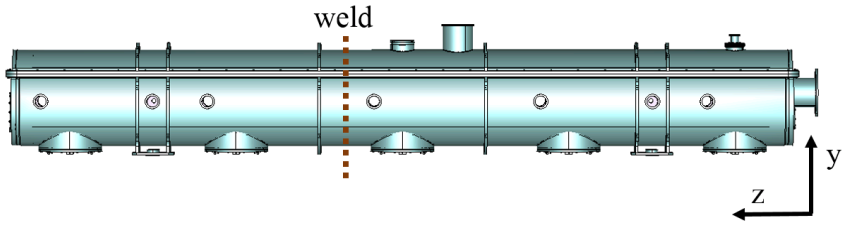

Fig. 9: The weld position at the vacuum vessel

where l is the length of the vessel. The measurements show a small contribution to the magnetic field inside the vessel due to magnetization (less than 1/3 of the ambient magnetic field).

6 Measurements in the vicinity of the weld

Placing the magnetic probe in the vicinity of the central weld on top of the shield, measurements were collected on the outer surface and the surrounding space outside the vessel with an increment of $5\,\mathrm{cm}$. Unfortunately it was not possible to collect these measurements in the interior of the vessel, however similar results would be expected inside the vessel. The results are shown in figure 11a. To enhance the image resolution, 2D cubic interpolation was used. The results are shown in figure 11b. As can be observed from the measurements, the field values drop to

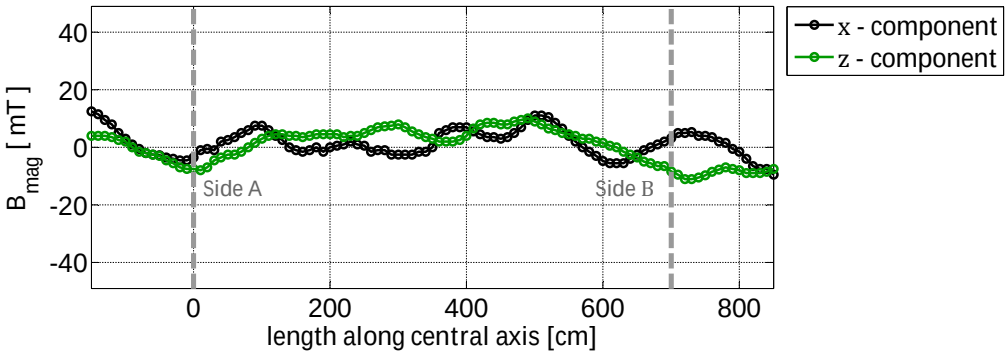

Fig. 10: The **x** and **z** component of the magnetization field B_{mag} as calculated by equation 1.

ambient magnetic field values in less than $10\,\mathrm{cm}$ away from the weld with a maximum value of $80\,\mu\mathrm{T}$ on the weld. The warm magnetic shield will be situated very close to the inner surface of the vessel and it will be lying in the region of the high magnetic field induced by the weld. The weld might enhance or decrease the shielding efficiency depending on the final orientation of the earth magnetic field with respect to the vessel. In any case the field remains low and since the warm shield has a thickness of $3\,\mathrm{mm}$ there is no risk of saturation of the magnetic material.

7 Measurements on the perpendicular axes of the vessel

In order to get a better picture of the magnetic field inside the vessel, measurements have been taken on paths perpendicular to the central axis in 5 different positions (red lines in figure 4). The results are provided for all the 5 axes and for the **x, y** and **z** components of the field as well as its absolute value in figures 12 and 13. The holes at the side of the vessel provided a good way to reach the interior (see figure 2c). The measurements show that very close to the short tubes just outside the holes the **x** and **z** components show a small increase in field. However it is highly localized and just comparable to the ambient magnetic field with no practical consequence.

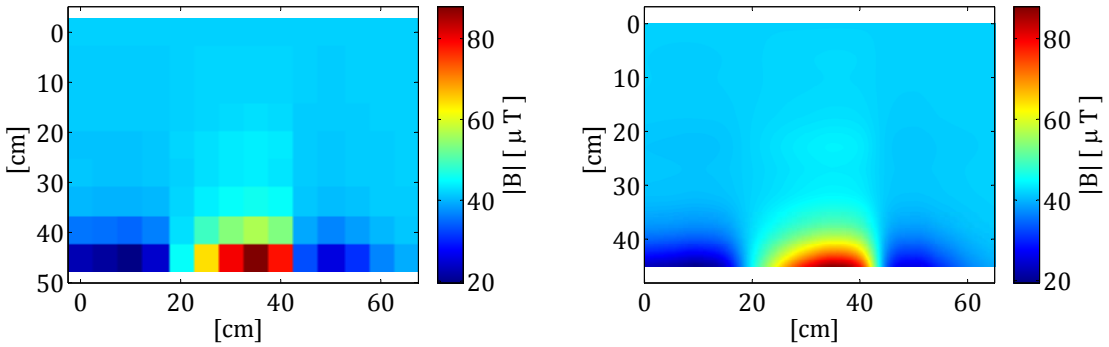

(a) measured data

(b) interpolated data (2D cubic interpolation)

Fig. 11: Measurement of the magnetic field in a plane perpendicular to the vacuum vessel, parallel to central axis outside of the vessel. The weld is located exactly at the point of maximum field (x: $35\,\mathrm{mm}$, y: $35\,\mathrm{mm}$)

8 Conclusions

Detailed magnetic measurements have been realised on the empty and closed vacuum vessel for the High-Gradient cryomodule. The shielding efficiency of the vessel is limited to a shieding

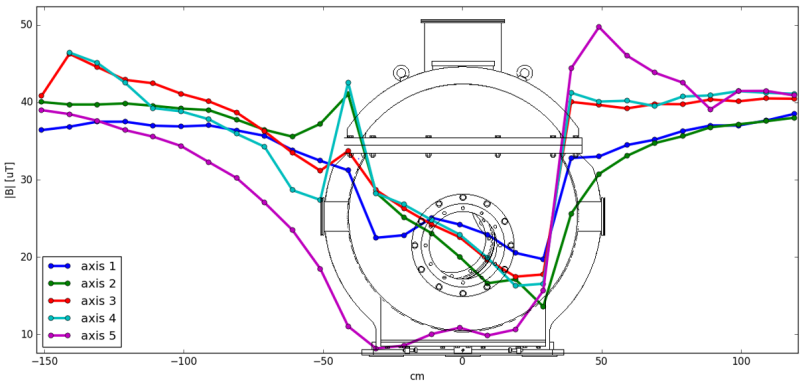

Fig. 12: Absolute value of the magnetic field along the various paths across the side openings of the vacuum vessel (see red lines on figure 4a and 4b)

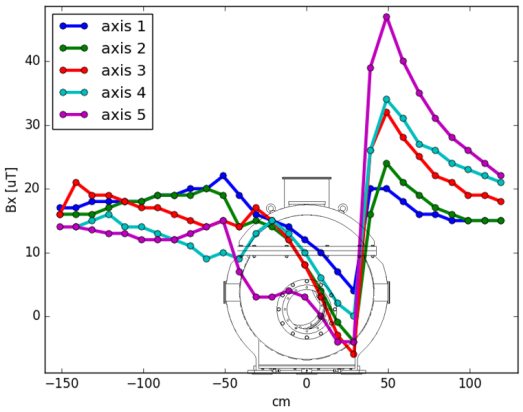

(a) **x**-component

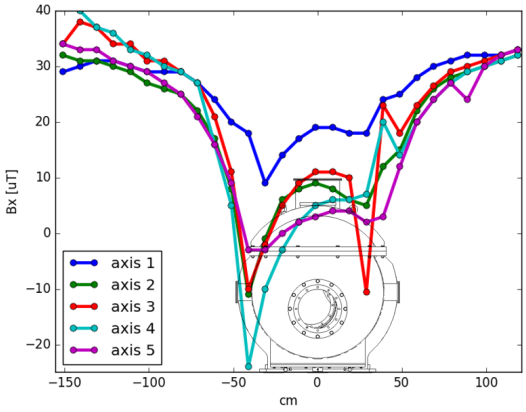

(b) **y**-component

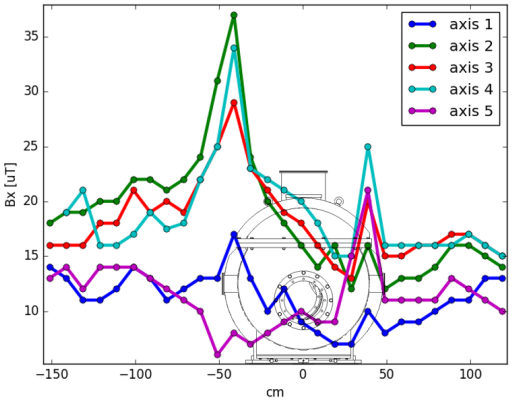

(c) **z**-component

Fig. 13: The **x, y** and **z** components of the magnetic field along the various side axes of the vacuum vessel through the side holes (see red lines on figure 4a and 4b).

factor between 2 and 3. By rotating the vessel, an effort has been made to measure the field induced by the magnetization of the vessel. The results show very low magnetization in the **x** and **z** components of the field which combined give a magnetization field with a mean value of $13\,\mu\mathrm{T}$, thus there is no need for demagnetization of the vessel.

9 Acknowledgment

This project has received funding from the European Union's Horizon 2020 Research and Innovation programme under Grant Agreement No 730871.

References

[1] Bartington Instruments, http://www.bartington.com/Literaturepdf/Datasheets/Mag-03%20DS0013.pdf

[2] World Magnetic Model, https://www.ngdc.noaa.gov/geomag-web/#igrfwmm